The Astrophysical Journal, 890:70 (14pp), 2020 February 10 https://doi.org/10.3847/1538-4357/ab6a1a
© 2020. The American Astronomical Society. All rights reserved.

Studying the Anisotropy of Compressible Magnetohydrodynamic Turbulence by Synchrotron Polarization Intensity

Ru-Yue Wang[1,2], Jian-Fu Zhang[1,2], and Fu-Yuan Xiang[1]
[1] Department of Physics, Xiangtan University, Xiangtan, Hunan 411105, People's Republic of China; jfzhang@xtu.edu.cn
[2] Guizhou Provincial Key Laboratory of Radio Astronomy and Data Processing, Guiyang, Guizhou 550025, People's Republic of China
Received 2019 November 15; revised 2020 January 5; accepted 2020 January 7; published 2020 February 13

Abstract

Based on statistical analysis of synchrotron polarization intensity, we study the anisotropic properties of compressible magnetohydrodynamic (MHD) turbulence. The second-order normalized structure function, quadrupole ratio modulus, and anisotropic coefficient are synergistically used to characterize the anisotropy of the polarization intensity. On the basis of predecomposition data cubes, we first explore the anisotropy of the polarization intensity in different turbulence regimes and find that the most significant anisotropy occurs in the sub-Alfvénic regime. Using postdecomposition data cubes in this regime, we then study the anisotropy of the polarization intensity from Alfvén, slow, and fast modes. The statistics of the polarization intensity from Alfvén and slow modes demonstrate the significant anisotropy, while the statistics of the polarization intensity from fast modes show isotropic structures. This is consistent with earlier results provided in Cho & Lazarian. As a result, both quadrupole ratio modulus and anisotropic coefficient for polarization intensities can quantitatively recover the anisotropy of underlying compressible magnetohydrodynamic turbulence. The synergistic use of the two methods helps enhance the reliability of the magnetic field measurement.

Unified Astronomy Thesaurus concepts: Interstellar magnetic fields (845); Magnetohydrodynamics (1964); Interstellar synchrotron emission (856)

1. Introduction

Magnetohydrodynamic (MHD) turbulence is ubiquitous in astrophysical environments (see Armstrong et al. 1995; Ferrière 2001; Elmegreen & Scalo 2004), and has a profound impact on many key astrophysical processes, such as the formation of stars (Mac Low & Klessen 2004; McKee & Ostriker 2007), the propagation and acceleration of cosmic rays (Yan & Lazarian 2008), heat conduction (Narayan & Medvedev 2001), and turbulent magnetic reconnection (Lazarian & Vishniac 1999, hereafter LV99). Thus, studying the properties of MHD turbulence is necessary for a thorough comprehension of key astrophysical progresses.

Magnetohydrodynamic turbulence has long been understood to be isotropic (Iroshnikov 1964; Kraichnan 1965; Shebalin et al. 1983). However, significant progress was made by Goldreich & Sridhar (1995), henceforth GS95, in understanding the properties of incompressible MHD turbulence, which was predicted to be anisotropic by considering relative motions of eddies parallel and perpendicular to the magnetic field directions. The anisotropies of the turbulence are related to the eddy scales, that is, the smaller the eddy scale, the more elongated the anisotropic structures of the turbulence. These relations, predicted by GS95, have been confirmed numerically (Cho & Vishniac 2000; Maron & Goldreich 2001; Cho & Lazarian 2002; hereafter CL02; Cho & Lazarian 2003; hereafter CL03). It is worth pointing out that the GS95 theory was applicable for the local system of reference defined by the direction of the local mean magnetic field surrounding the eddies (LV99; Cho & Vishniac 2000; Cho et al. 2002). This definition provides an important basis for understanding the critical balance condition, the scale-dependent anisotropy, and turbulent reconnection theory. The GS95 theory focused on incompressible MHD turbulence, which was extended to compressible ones (CL02 and CL03). The anisotropies of compressible MHD turbulence were explored in the subsequent numerical simulation (Matthaeus et al. 1996), which opened the way for numerical simulation of the compressibility of MHD turbulence. An important work of compressible MHD turbulence was carried out by CL02, who developed and tested the technique of separating different MHD modes. By decomposing the MHD turbulence modes, they found that Alfvén and slow modes have scale-dependent GS95 anisotropy, while the fast mode is isotropic.

In fact, the compressible MHD turbulence is involved in density and magnetic field fluctuations. The plasma parameter $\beta = P_{\rm gas}/P_{\rm mag}$ is used to characterize the compressibility of MHD turbulence, where $P_{\rm gas}$ and $P_{\rm mag}$ are gas and magnetic pressures, respectively. By introducing the Alfvénic and sonic Mach numbers,

$$M_{\rm A} = \left\langle \frac{|\boldsymbol{v}|}{v_{\rm A}} \right\rangle, \quad \text{and} \quad M_{\rm s} = \left\langle \frac{|\boldsymbol{v}|}{c_{\rm s}} \right\rangle, \tag{1}$$

respectively, we have $\beta = 2M_{\rm A}^2/M_{\rm s}^2$. Here, $\boldsymbol{v}$ is the gas velocity, $v_{\rm A} = |\boldsymbol{B}|/\sqrt{4\pi\rho}$ is Alfvénic velocity, and $c_{\rm s}$ is the sound speed. The high-β regime indicates a gas-pressure-dominated plasma, whereas the low-β regime is a magnetic-pressure-dominated one. The incompressible regime formally corresponds to $\beta \sim \infty$, and the compressible one to the low-β regime.

Although a numerical simulation is a great tool for exploring the properties of MHD turbulence, the currently available 3D simulations are limited by numerical resolutions, with the Reynolds number up to $\sim 10^5$ less than the Reynolds number at least 10^8 of real astrophysical fluids. Therefore, measurements of the interstellar medium (ISM) turbulence are important for studying properties of ISM, gauging the cosmic microwave background foregrounds, and predicting the propagation of cosmic rays. Obviously, to develop an effective method based on observations is very promising for exploring the properties of turbulent fluctuations.

Based on an analytical description, Lazarian & Pogosyan (2012, henceforth LP12) made the first step into employing statistics of synchrotron intensity fluctuations to recover the properties of MHD turbulence. They predicted that (1) synchrotron intensity fluctuations are anisotropic with the elongated structure along the direction of magnetic field; (2) anisotropies of synchrotron fluctuations are dominated by the quadrupole component, and the quadrupole ratio, i.e., the ratio between quadrupole and monopole parts, is sensitive to the compressibility of underlying turbulence; (3) synchrotron intensity correlations are very weakly dependent on the spectral index of relativistic electrons. These theoretical predictions were tested and verified numerically by Herron et al. (2016) using MHD turbulence simulations. In addition, LP12 also found that the quadrupole ratio moduli of synchrotron intensity from three (Alfvén, slow, and fast) modes show different levels of anisotropy related to Alfvénic Mach numbers, which should be tested further. The advantage of using synchrotron intensity fluctuations to study MHD turbulence is free from the influence of Faraday rotation. However, we all know that this technique is not applicable to the line-of-sight magnetic field measurements.

In view of the powerful and abundant polarization observations, the traditional Faraday rotation synthesis or Faraday tomography (Burn 1966; Brentjens & de Bruyn 2005) has been popularly used in studies of the properties of the magnetic field by combining synchrotron polarization with the Faraday rotation effect. This method was recently applied to polarized observational data and provides significant insight into magnetic field structures of galaxies (see Fletcher et al. 2011; Beck & Wielebinski 2013; Haverkorn 2015 for a review) and the properties of the ISM (Jelić et al. 2015; Van Eck et al. 2017; Dickey et al. 2019). An apparent limitation of the Faraday tomography is related to its treatment of magnetic turbulence. In particular, the estimation of the line-of-sight magnetic field through the Faraday depth is ambiguous due to magnetic field reversals along the line of sight. With the purpose of measuring the properties of MHD turbulence, statistical techniques of synchrotron polarization gradient, i.e., the gradient of polarized vector, have been applied to determining the sonic Mach number of the interstellar turbulence (Gaensler et al. 2011; Burkhart et al. 2012). Very recently, more sophisticated constructions of synchrotron diagnostics have been derived in Herron et al. (2018) to feasibly explore the magnetized ISM.

Taking synchrotron polarization fluctuations into account, Lazarian & Pogosyan (2016, henceforth LP16) introduced two important new techniques, i.e., polarization spatial analysis and polarization frequency analysis, to obtain the properties of magnetic turbulence, such as the power spectral index and correlation scale. These two techniques consider polarization fluctuations as a function of the spatial separation of the direction of the measurements and wavelength for the same line of sight, respectively. The theoretical predictions presented by LP16 have been successfully tested by Zhang et al. (2016, 2018). With the modern understanding of MHD turbulence theory (GS95) and analytical theoretical description of synchrotron intensities (LP12) and polarization intensities (LP16), Lazarian & Yuen (2018) developed a new (scalar quantity) gradient technique of synchrotron polarization intensities that is different from the gradient of polarization vector provided by Gaensler et al. (2011) to trace the direction of mean magnetic fields. The new gradient technique originates from the relation between the magnetic field direction and synchrotron gradients according to the modern understanding of the fundamental theory of magnetic turbulence, i.e., the eddies that align with the local magnetic field that surrounds the eddies. This technique has been generalized from the sub-Alfvénic to the super-Alfvénic turbulence regime in terms of the multifrequency measurement (Zhang et al. 2019a). By analogy to anisotropies for synchrotron intensity fluctuations (LP12), LP16 predicted that polarization intensity fluctuations should show a similar behavior, recovering the underlying magnetic field fluctuations.

It is obvious that not only can recovering the anisotropy of MHD turbulence explore the structure of the eddies, but it can also trace the direction of the mean magnetic field. In addition, studying compressibility allows us to understand the relations between the turbulent magnetic filed and densities better. As mentioned above, a large number of the properties of compressible MHD turbulence are derived from a direct numerical simulation. The current numerical capabilities are not sufficient to simulate a real astrophysical environment, however; we do not know to what extent the properties and laws based on finite numerical simulations are correct. This motivates us to explore the properties of compressible MHD turbulence using mimicked polarization observations. We expect to know whether statistical analysis techniques of polarization intensities can reveal the properties of the anisotropy and compressibility of MHD turbulence.

The structure of the paper is as follows. In Section 2 we provide theoretical descriptions including MHD turbulence basics, synchrotron radiative processes, and measurement techniques of synchrotron polarization fluctuations. Section 3 presents the procedure of the numerical simulation of MHD turbulence. Anisotropies of polarization intensity are presented in Section 4 for the mode predecomposition scenario and in Section 5 for the mode postdecomposition case. Discussion and a brief summary are given in Sections 6 and 7, respectively.

2. Theoretical Descriptions

2.1. Fundamental of MHD Turbulence

The modern MHD turbulence theory states a collection of anisotropic eddies in the presence of a strong magnetic field (GS95), the direction of which is aligned with the major axis of the eddies. In general, this alignment law can be retained only when the energy of the magnetic field over the volume of the eddy is equivalent to or higher than the kinetic energy of the eddy. The Alfvénic Mach number mentioned above can quantificationally characterize this relation. This parameter can be used to describe different MHD regimes. The incompressible MHD turbulence by GS95 corresponds to $M_{\rm A} \sim 1$, for example. Under the condition of a critical balance, i.e., $v_l l_\perp^{-1} = V_{\rm A} l_\parallel^{-1}$, where v_l is the fluctuation velocity at the scale l, with $l_\parallel$ and $l_\perp$ indicating parallel and perpendicular scales of the eddies, respectively, the derived relation of

$$l_\parallel \propto l_\perp^{2/3} \tag{2}$$

characterizes the anisotropy of MHD turbulence.

The generalization of the GS95 theory to $M_{\rm A} < 1$ and $M_{\rm A} > 1$ was provided in LV99 and Lazarian (2006). In the case of the $M_{\rm A} < 1$, when the turbulence is driven with sub-Alfvénic velocities at an injection scale $L_{\rm inj}$, there is a range of weak turbulence that spans from $L_{\rm inj}$ to the transition scale $l_{\rm trans} = L_{\rm inj} M_{\rm A}^2$. The strong sub-Alfvénic turbulence is present on the

scales smaller than $l_{\rm trans}$. The eddies of magnetic turbulence are more elongated along the magnetic field compared to the original GS95 anisotropy (see Equation (2)). Over the inertial range of $[l_{\rm trans}, l_{\rm diss}]$, where $l_{\rm diss}$ is the turbulence dissipation scale, the relation between the extended eddy scale along the magnetic field $l_\parallel$ and the transversal eddy scale $l_\perp$ is

$$l_\parallel \approx L_{\rm inj}^{1/3} l_\perp^{2/3} M_{\rm A}^{-4/3}, \tag{3}$$

when $M_{\rm A} = 1$ returns to the original GS95 relation. What can be obtained in the case of $M_{\rm A} > 1$ corresponds to super-Alfvénic turbulence $V_{\rm L} > V_{\rm A}$. For the limiting case of $M_{\rm A} \gg 1$, because the weak magnetic field has a marginal influence on MHD turbulence, the turbulence at scale close to $L_{\rm inj}$ scale has an essentially hydrodynamic Kolmogorov property, i.e., $v_l = V_{\rm L}(l/L_{\rm inj})^{1/3}$. The hydrodynamic properties of cascade processes have been changed at the scale $l_{\rm A} = L_{\rm inj} M_{\rm A}^{-3}$, where the turbulent velocity is equal to the Alfvén velocity $v_l = V_{\rm A}$ (Lazarian 2006). In the inertial range of $[l_{\rm A}, l_{\rm diss}]$, the super-Alfvénic turbulence again shows the characteristics of the GS95 anisotropy.

The GS95 theory developed in the study of incompressible turbulence serves as a guide in the later exploration of compressible MHD turbulence. The applicability of the model of real compressible turbulence was obtained in numerical simulations (Lithwick & Goldreich 2001, CL02 and CL03). Specifically, CL02 and CL03 presented a technique of decomposing MHD turbulence into three modes, i.e., Alfvén, slow, and fast modes, which made a great contribution to the development of MHD turbulence. They demonstrated that while the density is greatly modified as a result of the compressibility, the magnetic and velocity fluctuations of Alfvén and slow modes are only marginally different from the incompressible case. Meanwhile, numerical simulations show that the amount of energy in fast modes is smaller than that in Alfvén and slow modes (CL02, and Kowal & Lazarian 2010). Among them, Alfvén modes follow Kolmogorov spectrum ($l_\parallel \propto l_\perp^{2/3}$) and are compatible with the GS95 anisotropic model, while slow modes ($l_\parallel \propto l_\perp^{2/3}$) sheared by Alfvén modes are likely to evolve passively, and fast modes have isotropic properties ($l_\parallel \propto l_\perp$).

2.2. Synchrotron Radiative Processes

The relativistic electrons that merged into the magnetic field are accelerated by the Lorentz force, resulting in the production of synchrotron radiation. Because synchrotron fluctuations carry the information of turbulent magnetic fluctuations, developing a statistical technique related to synchrotron observations is a natural way for the study of MHD turbulence. We assume a homogeneous and isotropic power-law energy distribution of relativistic electrons,

$$N(E)dE = KE^{2\alpha-1}dE, \tag{4}$$

where N is the number density of relativistic electrons with the energy between E and $E + dE$, K is the normalization constant, and α is the spectral index of the electrons.

The synchrotron emission intensity as a function of radiative frequency ν is given by (Ginzburg & Syrovatskii 1965)

$$I(\nu) = \frac{e^3}{4\pi m_{\rm e} c^2} \int_0^L \frac{\sqrt{3}}{2-2\alpha} \Gamma\left(\frac{2-6\alpha}{12}\right)\Gamma\left(\frac{22-6\alpha}{12}\right) \times \left(\frac{3e}{2\pi m_{\rm e}^3 c^5}\right)^{-\alpha} K B_\perp^{1-\alpha} \nu^\alpha dL, \tag{5}$$

where Γ indicates the gamma function, $B_\perp$ represents the strength of the magnetic field perpendicular to the line of sight, and L is the integral length along the line of sight. Other parameters (e, $m_{\rm e}$, and c) keep their usual meanings.

By means of the synchrotron intensity provided in Equation (5) and the fraction polarization degree (p), the linearly polarized intensity can be calculated by

$$\mathrm{PI} = I \times p = I \times \frac{3-3\alpha}{5-3\alpha}. \tag{6}$$

The Stokes parameters Q and U are related to the polarization intensity by $Q = \mathrm{PI}\cos 2\psi$ and $U = \mathrm{PI}\sin 2\psi$. From the view point of an observation, the polarization intensity PI and the polarization angle ψ (measured anticlockwise from north) are an intuitive measurement for the linearly polarized emission (Hamaker & Bregman 1996) and are given by

$$\mathrm{PI} = \sqrt{Q^2 + U^2} \text{ and } \psi = \frac{1}{2}\arctan\frac{U}{Q}. \tag{7}$$

Moreover, we can define the complex polarization vector as $\boldsymbol{P} = Q + iU$, by which the polarization intensity is written as the complex modulus of $|\boldsymbol{P}|$ and the complex argument as 2ψ in the Q–U plane. With the consideration of the Faraday rotation effect, the polarization angle is expressed as $\psi = \psi_0 + \mathrm{RM}\lambda^2$, where λ is the wavelength of synchrotron radiation, and the rotation measure is given by $\mathrm{RM} = 0.81\int_0^L n_{\rm e} B_\parallel\, dz$ rad m^{-2}, where $n_{\rm e}$ is the number density of thermal electrons and $B_\parallel$ is the strength of the magnetic field parallel to the line of sight.

2.3. Statistical Measure Techniques

To extract the properties of MHD turbulence, basic statistical tools, such as the power spectrum, the power density spectrum, the correlation function, and the structure function, are adopted. In this paper, both the structure function and a new quadrupole ratio for synchrotron polarization intensities are used to explore the anisotropy of compressible MHD turbulence.

Based on LP12, the normalized correlation function of synchrotron polarization intensity is written as

$$\xi_{\rm PI}(\boldsymbol{R}) = \frac{\langle \mathrm{PI}(\boldsymbol{X})\mathrm{PI}(\boldsymbol{X}+\boldsymbol{R})\rangle - \langle \mathrm{PI}(\boldsymbol{X})\rangle^2}{\langle \mathrm{PI}(\boldsymbol{X})^2\rangle - \langle \mathrm{PI}(\boldsymbol{X})\rangle^2}, \tag{8}$$

where $\boldsymbol{X} = (x, y)$ denotes a two-dimensional position vector, and $\boldsymbol{R}$ is the separation vector between any two points on the plane of the sky. By analogy of the formula of LP12, the structure function of the synchrotron polarization intensity is given by

$$D_{\rm PI}(\boldsymbol{R}) = \langle (\mathrm{PI}(\boldsymbol{X}) - \mathrm{PI}(\boldsymbol{X}+\boldsymbol{R})^2\rangle. \tag{9}$$

Alternatively, the normalized structure function of the polarization intensity can be obtained by

$$\tilde{D}_{\rm PI} = 2(1 - \xi_{\rm PI}), \tag{10}$$

according to Equation (8). By Equation (10), the quadrupole ratio for synchrotron polarization intensities is defined by LP12,

$$\frac{\tilde{M}_2(R)}{\tilde{M}_0(R)} = \frac{\int_0^{2\pi} e^{-2i\phi}\tilde{D}_{\rm PI}(R,\,\phi)d\phi}{\int_0^{2\pi}\tilde{D}_{\rm PI}(R,\,\phi)\,d\phi}, \tag{11}$$

where R is the radial separation between two points, and ϕ represents the polar angle. The quadrupole ratio is used to reveal the anisotropy of MHD turbulence.

In addition, we can employ a diagnostic of the anisotropic coefficient to quantitatively characterize the anisotropy of the turbulence. Specifically, we consider two measurement directions perpendicular to each other from polarization intensities and define their ratio of the individual structure function,

$$\mathrm{AC} = \frac{\mathrm{SF}_\parallel}{\mathrm{SF}_\perp} = \frac{\langle|\mathrm{PI}_\parallel(x + r_\parallel) - \mathrm{PI}_\parallel(x)|^2\rangle}{\langle|\mathrm{PI}_\perp(y + r_\perp) - \mathrm{PI}_\perp(y)|^2\rangle}, \tag{12}$$

as an anisotropic coefficient in dimensionless units, with the relation of $r = [r_\parallel^2 + r_\perp^2]^{1/2}$. Equation (12) indicates that the isotropy and anisotropy of the turbulence structure happened in the case of AC = 1 and that of AC far away from 1, respectively.

3. Simulation Methods and Data Generation

The third-order-accurate hybrid, essentially nonoscillatory code, is used to solve control equations of MHD turbulence as follows:

$$\partial\rho/\partial t + \nabla\cdot(\rho\boldsymbol{v}) = 0, \tag{13}$$

$$\rho[\partial\boldsymbol{v}/\partial t + (\boldsymbol{v}\cdot\nabla)\boldsymbol{v}] + \nabla p - \boldsymbol{J}\times\boldsymbol{B}/4\pi = \boldsymbol{f}, \tag{14}$$

$$\partial\boldsymbol{B}/\partial t - \nabla\times(\boldsymbol{v}\times\boldsymbol{B}) = 0, \tag{15}$$

$$\nabla\cdot\boldsymbol{B} = 0, \tag{16}$$

and simulates an emitting synchrotron radiation medium in a periodic box of the length of 2π. Here, $p = c_s^2\rho$ is the gas pressure, t is the evolution time of the fluid, $\boldsymbol{J} = \nabla\times\boldsymbol{B}$ is the current density, and $\boldsymbol{f}$ is a random driving force. In the simulation, the turbulence is driven by a random solenoidal driving force on large scales, and an isothermal equation of state is used to close the above equations. Furthermore, nonzero mean magnetic fields are set along the x-axis direction. The obtained data cubes with numerical resolution of 512^3, corresponding to different turbulence regimes, are listed in Table 1. These data cubes are mainly characterized by the Alfvénic and sonic Mach numbers.

The decomposition method of MHD modes provided by CL02 is used to decompose data cubes listed in Table 1 into Alfvén, slow, and fast modes.[3] The main procedures are given as follows:

$$\hat{\zeta}_{\rm f} \propto \left(1, +, \frac{\beta}{2}, +, \sqrt{D}\right)(k_\perp\hat{\boldsymbol{k}}_\perp) + \left(-, 1, +, \frac{\beta}{2}, +, \sqrt{D}\right)(k_\parallel\hat{\boldsymbol{k}}_\parallel), \tag{17}$$

[3] Here, each MHD mode is separated by the Fourier transformation related to the mean magnetic field. Because it is affected by the wandering of large-scale magnetic field and density inhomogeneities, this approach is applicable for the case of the sub-Alfvénic turbulence with a strong mean magnetic field and small perturbation. An improved procedure is to extend the CL03 decomposition into modes, in which each components of the local magnetic field is decomposed into orthogonal wavelets using discrete wavelet transformation (Kowal & Lazarian 2010). This method has more significant advantages in dealing with turbulent fluctuations of high amplitude such as trans-Alfvénic turbulence.

Table 1
Data Cubes with Numerical Resolution of 512^3 Generated in the Simulation of Compressible MHD Turbulence

Run	M_s	M_A	β	$\delta B_{\rm rms}/\langle B\rangle$	Turbulence Regime
1	9.92	0.50	0.005	0.465	Supersonic and sub-Alfvénic
2	6.78	0.52	0.012	0.463	Supersonic and sub-Alfvénic
3	4.46	0.55	0.030	0.467	Supersonic and sub-Alfvénic
4	3.16	0.58	0.067	0.506	Supersonic and sub-Alfvénic
5	0.87	0.70	1.295	0.579	Subsonic and sub-Alfvénic
6	0.48	0.65	3.668	0.614	Subsonic and sub-Alfvénic
7	7.02	1.76	0.126	4.606	Supersonic and super-Alfvénic
8	4.32	1.51	0.244	5.175	Supersonic and super-Alfvénic
9	3.11	1.69	0.591	5.254	Supersonic and super-Alfvénic
10	0.83	1.74	8.790	6.110	Subsonic and super-Alfvénic
11	0.45	1.72	29.219	6.345	Subsonic and super-Alfvénic

Note. $\delta B_{\rm rms}$ indicates the root mean square of random magnetic field, and $\langle B\rangle$ the regular magnetic field.

$$\hat{\zeta}_{\rm s} \propto \left(1, +, \frac{\beta}{2}, -, \sqrt{D}\right)(k_\perp\hat{\boldsymbol{k}}_\perp) + \left(-, 1, +, \frac{\beta}{2}, -, \sqrt{D}\right)(k_\parallel\hat{\boldsymbol{k}}_\parallel), \tag{18}$$

$$\hat{\zeta}_{\rm A} \propto -\hat{\boldsymbol{k}}_\perp\times\hat{\boldsymbol{k}}_\parallel, \tag{19}$$

where $D = \left(1 + \frac{\beta}{2}\right)^2 - 2\beta\cos^2\theta$ and $\cos\theta = \hat{k}_\parallel\cdot\hat{B}$. We only use the line-of-sight component of decomposed velocities to calculate the magnetic field mode components, resulting in three magnetic field modes,

$$B_{\rm (f,s,a),z} = [\mathcal{F}^{-1}(\mathcal{F}(\boldsymbol{B})\cdot\hat{\zeta}_{\rm f,s,a})](\hat{\zeta}_{\rm f,s,a}\cdot\hat{\zeta}_{\rm LOS}), \tag{20}$$

where $\mathcal{F}$ is the Fourier transform operator.

The data cubes decomposed by the method of CL02 are employed as input parameters of Equations (5) and (6) to reprocess the simulation to construct a synthetic map of synchrotron emission. Assuming the line of sight (z-axis) perpendicular to the direction of mean magnetic fields (x-axis), we can calculate $B_\perp$ in Equation (5) by $B_\perp = \sqrt{B_x^2 + B_y^2}$. The final synthetic synchrotron map is generated by the line-of-sight integral to simulate real observations.

4. Anisotropy of the Polarization Intensity for Predecomposition MHD Modes

Before decomposing compressible MHD turbulence modes, we explore in this section the anisotropy of predecomposition MHD modes by the statistics of the synchrotron polarized intensity. Using the different statistical techniques and data cubes listed in Table 1, we investigate how Mach numbers (Section 4.1) and radiation frequency (Section 4.2) affect the anisotropy of the polarized intensity, reflecting the anisotropy of MHD turbulence.

4.1. Effect of Mach Numbers

We employ Equation (6) to obtain a synthetic map of the synchrotron polarization intensity with the setting of $\alpha = -1$ and $\nu = 10$ GHz, corresponding to the weak Faraday rotation effect. It is known that the structure function is the most intuitive method to reflect the structure anisotropy. Here, we

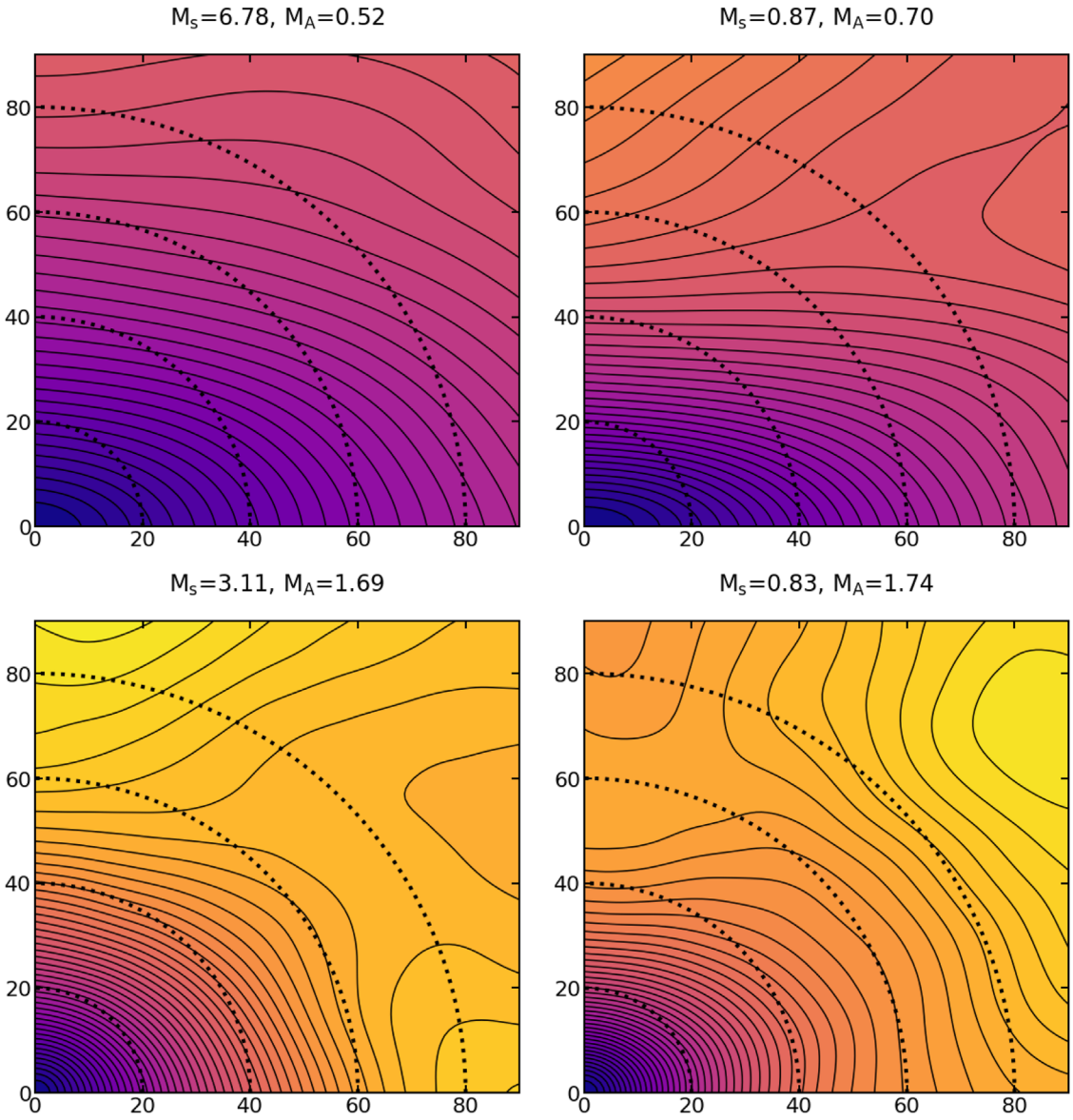

Figure 1. Images of the normalized structure function of synchrotron polarization intensities at different turbulence regimes. The dotted contour lines plotted in each panel denote isotropy.

focus mainly on using the second-order normalized structure function (see Equation (10)) to reveal the anisotropy of the polarization intensity at different turbulence regimes. The resulting contour maps of the normalized structure function of the polarization intensity are shown in Figure 1 at supersonic and sub-Alfvénic (left upper panel: $M_s = 6.78$, $M_A = 0.52$), subsonic and sub-Alfvénic (right upper panel: $M_s = 0.87$, $M_A = 0.70$), supersonic and super-Alfvénic (left lower panel: $M_s = 3.11$, $M_A = 1.69$), and subsonic and super-Alfvénic (right lower panel: $M_s = 0.83$, $M_A = 1.74$) regimes. The pixels of the map are in units of the code unit, and the dotted contour lines are plotted to indicate isotropy for the sake of comparison.

As shown in Figure 1, the solid contour lines are extended along the x-axis (horizontal) directions, which reflects the anisotropic structure of eddies whose major axis is aligned with the direction of the mean magnetic field. The right upper panel presents a more elongated structure of the normalized polarization intensity than that of the left upper panel, but the anisotropic structures in the right upper panel are destroyed on a large scale. Similarly, on a smaller scale (<60 pixels) than those of the upper panels, the right lower panel also presents slightly more extended structure than that of the left lower panel, both of which show that the structure is destroyed on a large scale. As a result, the anisotropy of the synchrotron polarization intensity is more sensitive to sub-Alfvénic than to super-Alfvénic turbulence. The reason is that sub-Alfvénic turbulence corresponds to stronger magnetic field fluctuation and produces more significant anisotropy. Although structures of polarized intensity have weak dependence on sonic Mach numbers, it can been seen that subsonic turbulence produces more anisotropic structure at small scales than supersonic turbulence. In addition, it may be that supersonic Mach number helps to form the structure of anisotropy on larger scales (see the left upper panel) due to the formation of shock waves.

To see the dependence of the anisotropy on Mach numbers more quantitatively, we apply the quadrupole ratio (see Equation (11)) to depict the anisotropy of the polarization

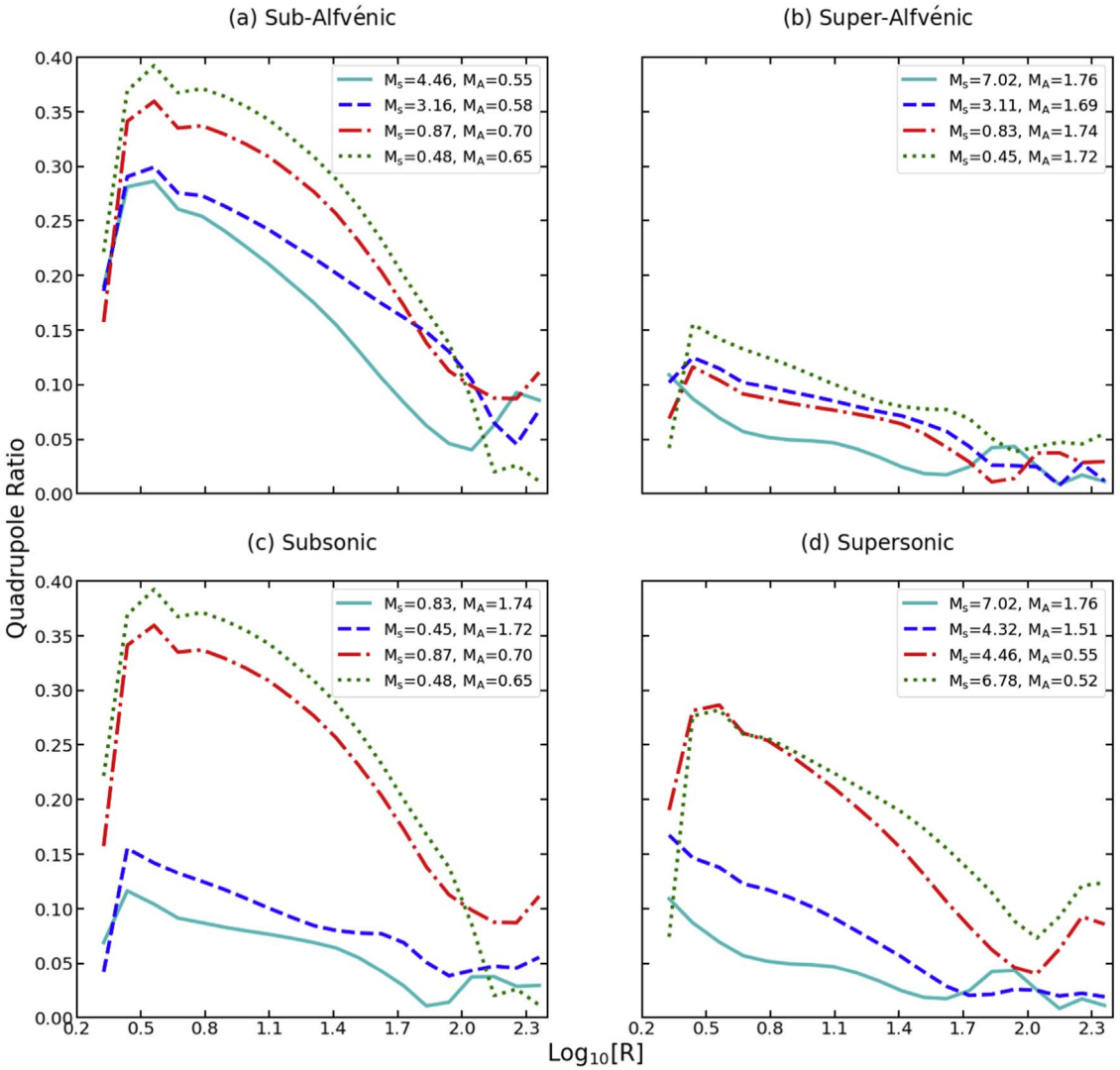

Figure 2. Quadrupole ratio modulus of the synchrotron polarization intensity as a function of the radial separation of maps at different turbulence regimes.

intensity. Based on the data listed in Table 1, quadrupole ratio moduli of the polarization intensity as a function of radial separation are plotted in Figure 2 at four different turbulence regimes. With increasing radial separation, quadrupole ratio moduli decrease and reach a minimum value with physical meaning at a scale of approximately 100 pixels. Between this scale and the injection scale of $\simeq$200 pixels, unstable curves reflect the phenomenon that the turbulence has not been fully developed. The curves of quadrupole ratio moduli show a trough at small scales of about 5 pixels, which is due to the existence of the discrete grid of pixels in 2D normalized structure function.

As for the upper panels of Figure 2, the quadrupole ratio modulus has the highest amplitude value of approximately 0.39 in the left panel, whereas the amplitudes are smaller than 0.15 for a wide range of radial separations in the right panel. It is easy to understand that quadrupole ratio moduli are sensitive to sub-Alfvénic Mach numbers, resulting in more anisotropy, while super-Alfvénic simulations present a weak anisotropy at small scales and almost isotropy at large scales.[4] As for the lower panels, the simulations related to sonic Mach numbers are separated into two parts, in which a high quadrupole ratio corresponds to low M_A, and a low quadrupole ratio to high M_A. The main reason may be that low M_A simulations have a stronger magnetic fluctuation and produce more magnetic-field-dominated anisotropy. It can also be seen that the quadrupole ratio moduli depend on sonic Mach numbers. The slope at large scales of the quadrupole ratio moduli for the sub-Alfvénic and subsonic simulation (left lower panel) is steeper than those for the sub-Alfvénic and supersonic simulation (right lower panel). The reason should be that increasing the sonic Mach number results in the formation of shock waves of fast fluid motions, which maintains smooth changes for the anisotropy of turbulence.

Alternatively, an additional statistical technique, called anisotropic coefficient, is used to test the anisotropy of the synchrotron polarization intensity. This technique does not only reflect the relative value of the component of the anisotropic structure, but also reveals the direction of the mean magnetic field. The anisotropic coefficients of the polarization intensity calculated by Equation (12) are plotted in Figure 3 using the same data cubes as in Figure 2. In each panel of Figure 3, the horizontal dashed line with AC = 1 represents the isotropy of

[4] It should be emphasized that the amplitude of the quadrupole ratio modulus is an important basis for judging anisotropy. According to our test using isotropic synthetic data generated in Zhang et al. (2016), we realize that if the mean amplitude $\lesssim$0.08, the structure of the map can be considered as isotropy.

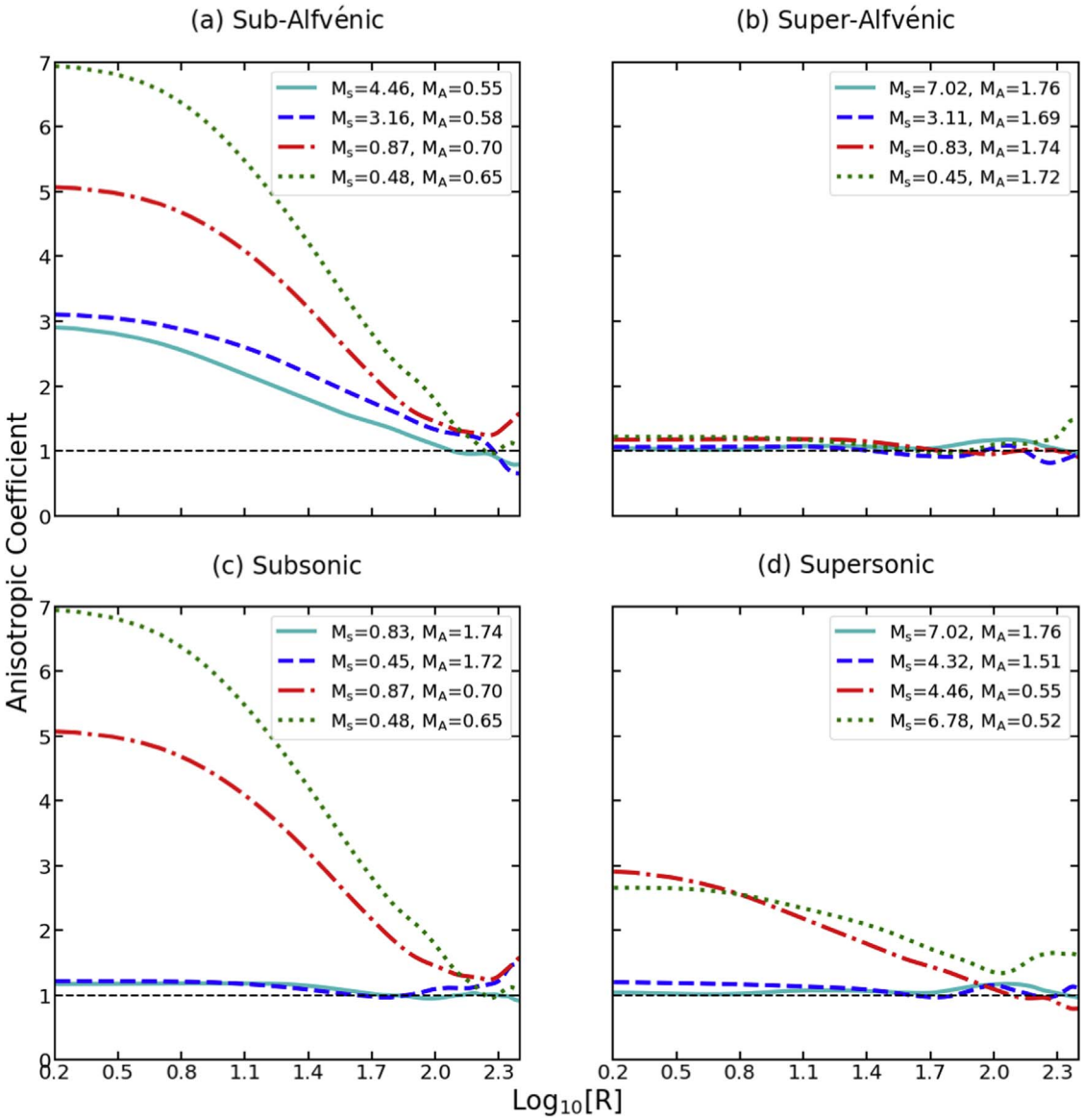

Figure 3. Anisotropic coefficient for synchrotron polarization intensity as a function of radial separation of maps at different turbulence regimes. The dashed line plotted in each panel corresponds to the anisotropic coefficient of 1, reflecting the isotropy properties of MHD turbulence.

the normalized structure function of the polarization intensity. As is seen in Figure 3, the anisotropic coefficients of polarization intensity show the scale-dependent anisotropy that decreases as the scale increases. It is clearly shown that the sub-Alfvénic simulation generates anisotropic coefficient values that far exceed those generated by the super-Alfvénic simulation (weak anisotropy). In other words, anisotropic coefficients are more sensitive to sub-Alfvénic Mach numbers, resulting in more significant anisotropy. In addition, we can see that the anisotropic coefficients in sub-Alfvénic regimes increase as the sonic Mach number decreases, which demonstrates the dependence of the anisotropic coefficient on sonic Mach number in sub-Alfvénic turbulence regimes. According to the anisotropic coefficient values (>1) shown in this figure, we derive the direction of the magnetic field in a horizontal (x-axis) direction.

4.2. Effect of Frequency

In this section we explore how radiative frequency affects the anisotropy of the synchrotron polarization intensity using the three methods mentioned above. All calculations are based on run 5 listed in Table 1 by setting different frequencies.

Figure 4 shows the contours of the normalized structure function of the polarization intensity at frequencies of $\nu = 1.4$, 0.5, 0.1, and 0.01 GHz. The dotted lines plotted in each panel denote the distribution of the isotropic structure for the sake of comparison. It can be clearly seen that structures of eddies are elongated along x-axis, i.e., the direction of the mean magnetic field. As the frequency decreases, the elongated anisotropic structures we can see from the figure move to a smaller scale, accompanied by a decrease in anisotropy levels, but the large-scale anisotropy structure is replaced by the chaotic one. The reason should be that as the frequency decreases, the Faraday rotation produces a stronger effect on the anisotropic structure, with the loss of correlation at a large scale. In any case, the Faraday rotation effect is no obstacle to studying anisotropy and tracing mean magnetic field directions.

Next, we use the quadrupole ratio modulus to explore the anisotropy of the synchrotron polarization intensity at frequencies

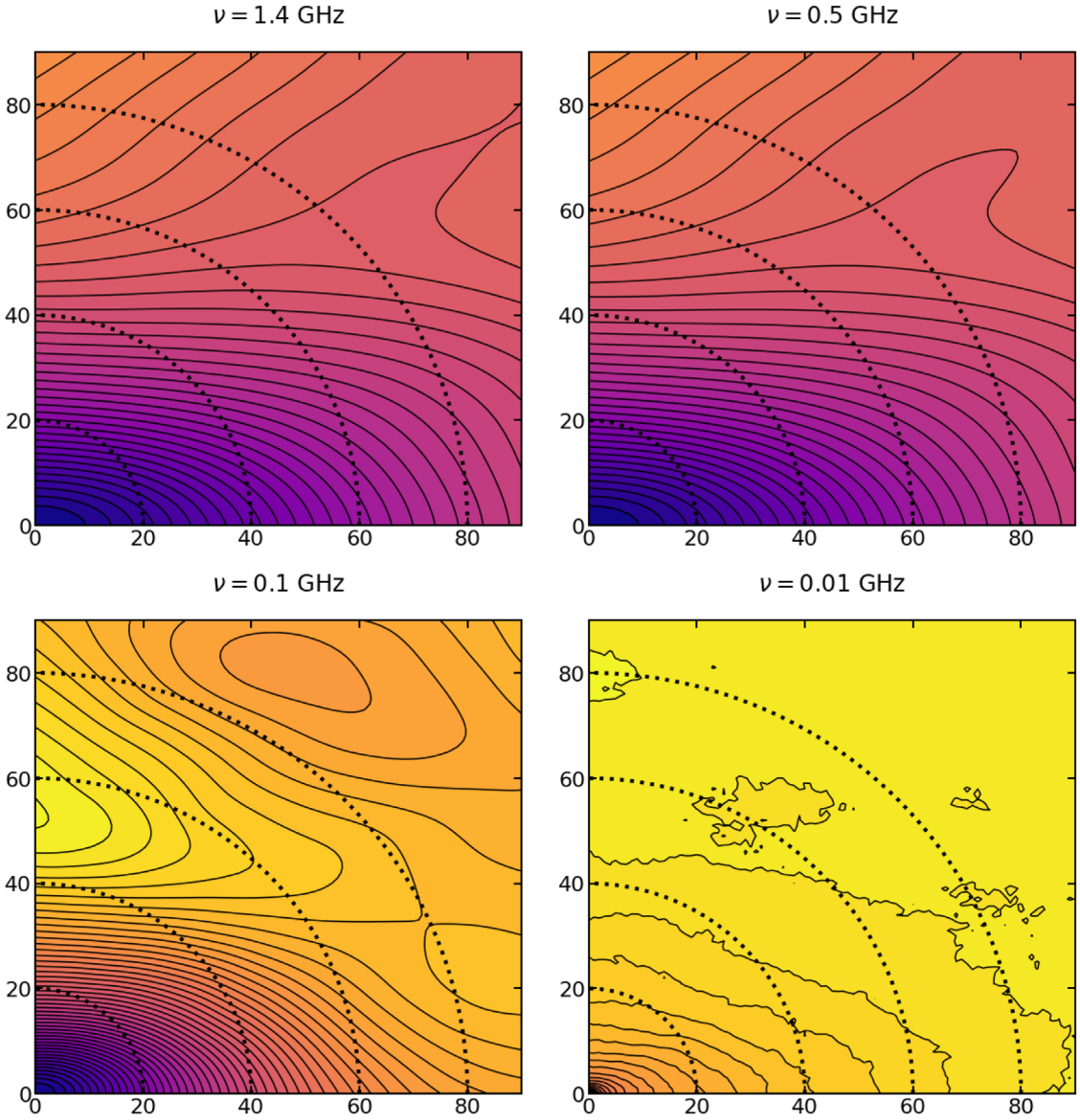

Figure 4. Contour maps of normalized structure function of synchrotron polarization intensity at different radiation frequencies. The dotted contour lines plotted in each panel indicate isotropy.

of $\nu = 1.4$, 0.5, 0.1, and 0.01 GHz. The quadrupole ratio modulus of the polarization intensity as a function of radial separation is shown in Figure 5. The amplitude of the quadrupole ratio modulus decreases with increasing radial separation, reflecting the anisotropic structures as more elongated at small scales. It can be seen that for the simulations plotted at 0.5 and 1.4 GHz, the quadrupole ratio moduli present almost the same distributions (changes occur at about 0.2 GHz according to our test), but the amplitude is significantly reduced for the simulation with the frequency of 0.01 GHz. As a result, the low-frequency Faraday rotation causes the anisotropy of the polarization intensity to decrease, which will be considered in detail in the future.

The influence of the frequency on the anisotropic coefficient is studied in Figure 6, in which the horizontal dotted line represents isotropy. It is shown that the anisotropic coefficient becomes small as the radial separation increases, which reflects the scale-dependent anisotropy. The dependence of the anisotropic coefficient on frequency is similar to the dependence shown in Figure 5. The difference is that the anisotropic coefficient can directly reveal the direction of the mean magnetic field, while the quadrupole ratio can reflect the anisotropic degree of the polarization intensity with high accuracy. Accordingly, combining the quadrupole ratio with the anisotropic coefficient can be very synergetic to study the anisotropy of the synchrotron polarization intensity.

5. Anisotropy of the Polarization Intensity for Postdecomposition MHD Modes

We now explore anisotropies of synchrotron polarized intensities for Alfvén, slow, and fast modes using the quadrupole ratio and anisotropic coefficient methods. As is shown in Section 4, because super-Alfvénic simulations show a weak anisotropy, only the sub-Alfvénic data listed in Table 1 are decomposed in this paper to study the anisotropic structure for the three modes.

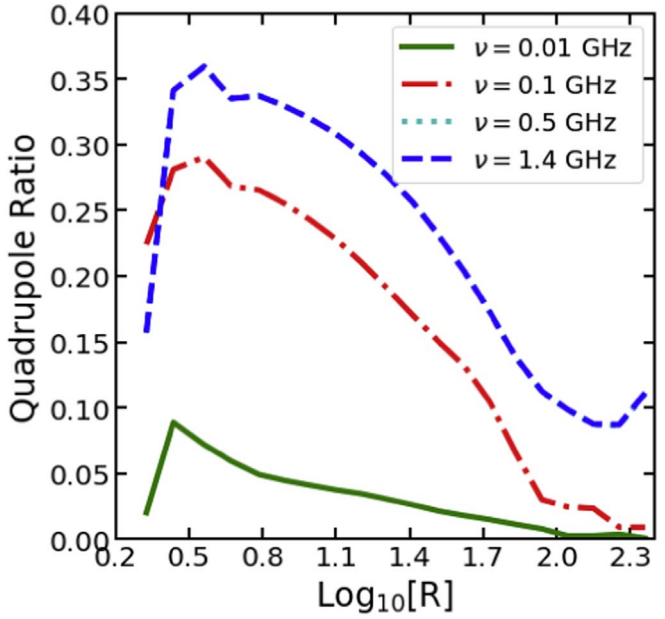

Figure 5. Quadrupole ratio modulus of the synchrotron polarization intensity as a function of radial separation at different frequencies.

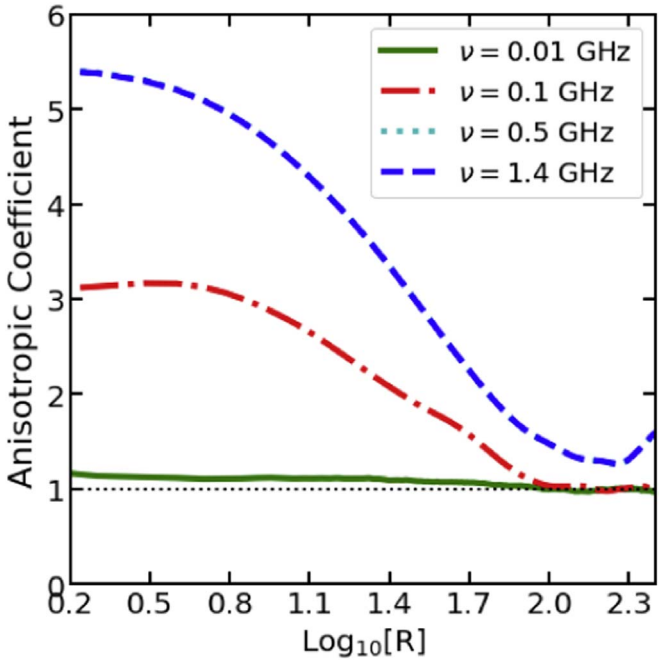

Figure 6. Anisotropic coefficient for the synchrotron polarization intensity as a function of radial separation of maps at different frequencies. The dotted line indicates isotropy of the map structure.

5.1. Influence of Mach Numbers

Using the parameters of the electron spectral index of $\alpha = -1$ and the frequency of $\nu = 10$ GHz, we show in Figure 7 quadrupole ratio moduli of polarized intensities calculated by Alfvén, slow, and fast modes. In the left and middle panels of this figure, the quadrupole ratio modulus is a decreasing function of the radial separation with the peak at approximately 6 pixels, a similar performance to those in the left upper panel of Figure 2, which reveals the scale-related anisotropy of Alfvén and slow modes. However, the quadrupole ratio moduli from Alfvén modes and slow modes vary in the dependence on M_s—the former are mild, while the latter are sensitive. The reason may be that these two modes have distinct intrinsic characteristics, i.e., incompressible Alfvén modes versus compressible slow modes. Concerning the simulations from slow modes, it can be seen that two curves (marked with $M_s = 0.48$, $M_A = 0.65$ and $M_s = 0.87$, $M_A = 0.70$) present larger amplitudes than others, which suggests that turbulent magnetic pressure dominates small M_s fluid pressure to stimulate anisotropic structure. Compared to Alfvén modes, most simulations for slow modes have a larger amplitude of quadrupole ratio moduli for the same set of simulations. Different from Alfvén and slow modes, the amplitudes of the quadrupole ratio modulus from fast modes (see right panel) have no scale dependencies and meet the anisotropic criterion of a mean amplitude lower than 0.08 mentioned above, which means the isotropy of the polarized intensity from fast modes.

We now adopt the anisotropic coefficient method to explore the degree of anisotropy for three modes, with the results plotted in Figure 8. It can be clearly seen in the left and middle panels that the anisotropic coefficient reflects the scale-dependent anisotropy well, and its magnitude larger than 1 decreases with increasing radial separation. As for distributions of the anisotropic coefficient, we find a larger magnitude of the anisotropic coefficient for slow modes than that of Alfvén modes in the same set of simulations. On the basis of Equation (12), we know that anisotropic structures of both Alfvén and slow modes are elongated along the x-axis, i.e., the direction of the mean magnetic field, which demonstrates that they have a similar anisotropic structure. In the case of the right panel, the magnitude of the fast-mode anisotropic coefficient is smaller than 1 but very close to 1, which indicates that an approximately isotropic structure of the polarization intensity should be aligned perpendicular to the mean magnetic field. Both Alfvén and slow modes dominate the composition of the compressible turbulence; the anisotropic structure of the polarized intensity for predecomposition MHD modes is confirmed in Section 4.

5.2. Influence of the Spectral Index

In this section we study the influence of relativistic electron spectral index on the anisotropy of polarized intensity at the fixed frequency of $\nu = 10$ GHz, on the basis of the MHD mode decomposition of run 5 listed in Table 1. First, the quadrupole ratio method is used to study the anisotropy of the synchrotron polarization intensity, and the results are shown in Figure 9. This figure shows the quadrupole ratio modulus for three modes as a function of radial separation by changing the spectral index of relativistic electrons. In general, the overall distributions of the quadrupole ratio modulus of the polarized intensity are similar to those of Figure 7. From this figure, we can see that the quadrupole ratio moduli for three modes marginally depend on the electron spectral index, the range of which covers the important cases in astrophysics we are aware of.

Using the anisotropic coefficient method, we now explore the influence of relativistic electron spectral index on the anisotropy of polarized intensities for three modes. Figure 10 shows the relation of the anisotropic coefficient and the radial separation at different spectral indices, from which we can see that the anisotropic coefficient of the polarized intensities from slow modes seems to be more sensitive than that from Alfvén modes. In particular,

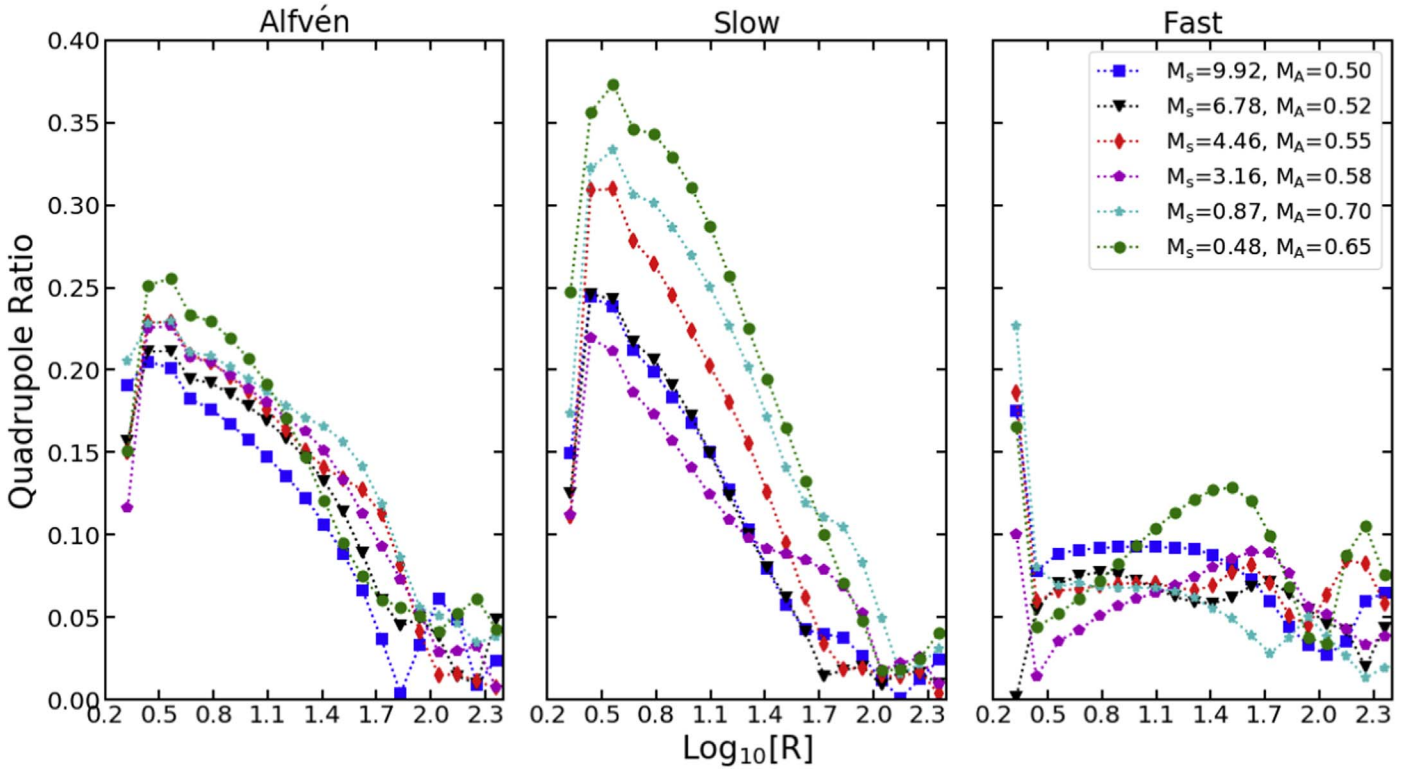

Figure 7. Quadrupole ratio moduli of the synchrotron polarization intensities for Alfvén, slow, and fast modes as a function of radial separation of maps in the sub-Alfvénic regime.

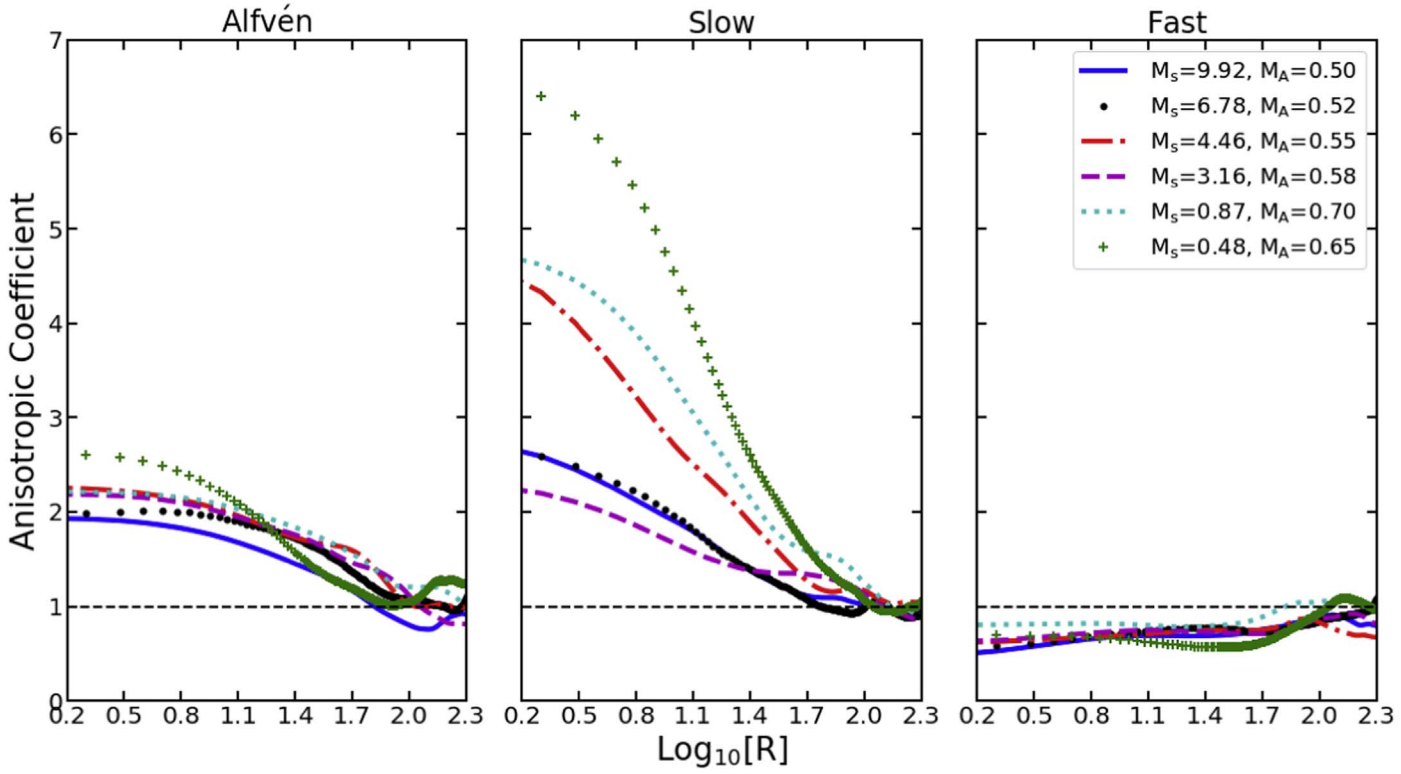

Figure 8. Anisotropic coefficients of the synchrotron polarization intensity for Alfvén, slow, and fast modes as a function of radial separation in the sub-Alfvénic regime. The dashed line plotted in each panel signifies isotropy.

the anisotropic coefficients from fast modes are insensitive to changes in radial separation. As a result, both the quadrupole ratio moduli and anisotropic coefficients from synchrotron polarization intensities marginally depend on the spectral index of relativistic electrons, the change of which does not prevent us from determining the anisotropy of magnetic turbulence.

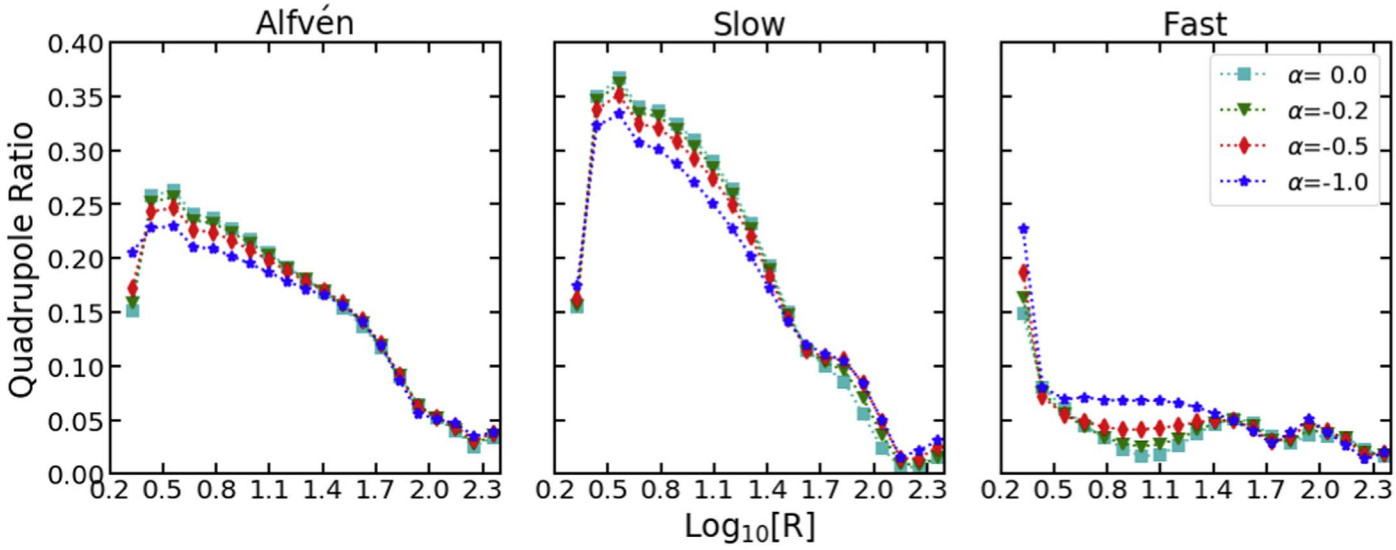

Figure 9. Influence of the relativistic electron spectral index on the quadrupole ratio moduli of the synchrotron polarization intensity for Alfvén, slow, and fast modes.

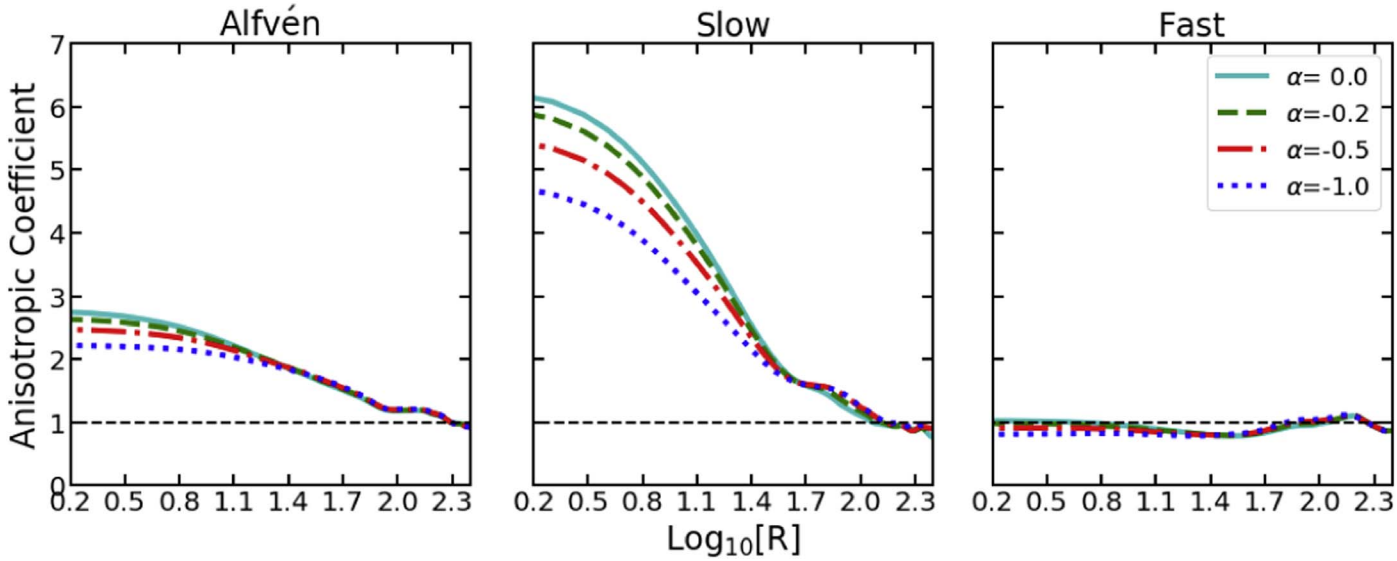

Figure 10. Influence of the relativistic electron spectral index on the anisotropic coefficients of the synchrotron polarization intensities for Alfvén, slow, and fast modes.

5.3. Influence of Frequency

The influence of the radiative frequency on the quadrupole ratio modulus of polarized intensities for three modes is explored in this section using the electron spectral index of $\alpha = -1$. Based on the MHD-mode decomposition of run 5 listed in Table 1, we adopt two statistical techniques mentioned above, i.e., the quadrupole ratio modulus and the anisotropic coefficient method, to reveal the anisotropy of MHD turbulence. Quadrupole ratio moduli for three modes as a function of radial separation are shown in Figure 11 at different frequencies. From this figure, we find that the quadrupole ratio moduli for three modes marginally depend on the frequency, while the quadrupole ratio modulus for slow modes has a smaller dependence on the frequency than those of other modes. In general, with decreasing the frequency, we expect the amplitude of the quadrupole ratio modulus to become smaller because the Faraday rotation effect becomes stronger at low frequencies. However, for the frequency ranges we study in this paper, the quadrupole ratio modulus for the slow mode does not change much. Therefore, the quadrupole ratio modulus with the larger amplitude from the slow mode provides a more reliable way to determine the anisotropy of magnetic turbulence than those of Alfvén and fast modes.

The anisotropy of the polarization intensities for three modes at different frequencies is plotted in Figure 12 by the anisotropic coefficient method. As is shown in this figure, the anisotropic coefficients of the polarized intensities for three modes show a behavior similar to those of Figure 11. Namely, the anisotropic coefficients for the slow mode are less sensitive to the frequency, while the anisotropic coefficients for the Alfvén and fast modes depend on the frequency. As a result, the low-frequency strong Faraday rotation effect slightly reduces the anisotropic degree of the polarization intensity, whose structures are elongated along the mean magnetic field direction for Alfvén and slow modes.

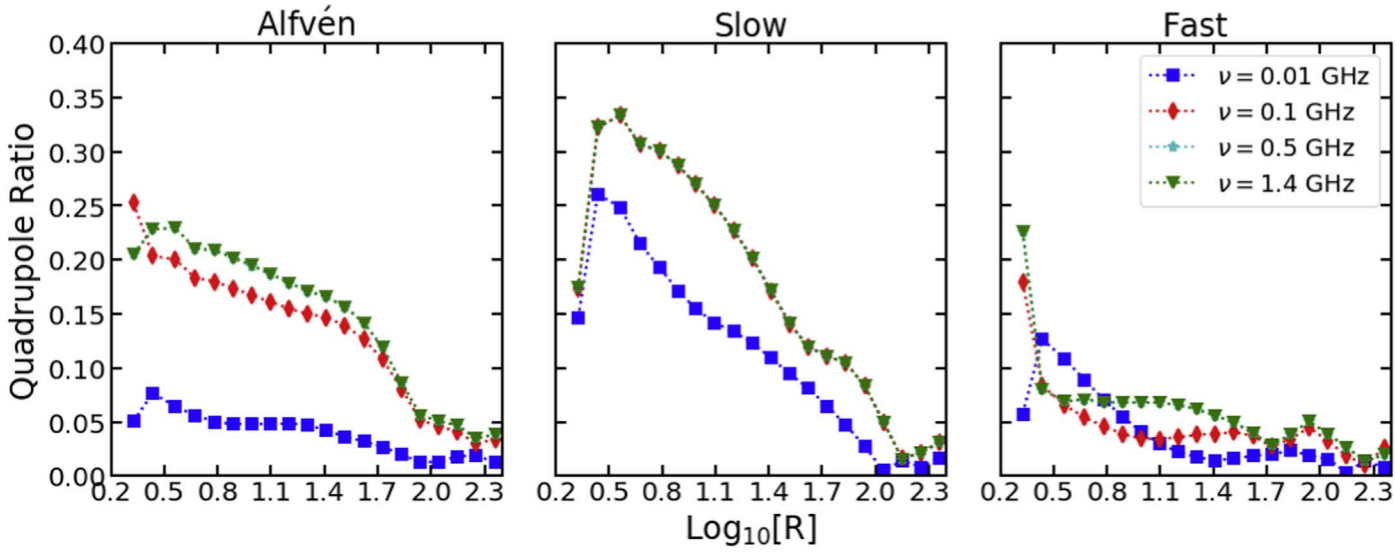

Figure 11. Influence of the radiation frequency on the quadrupole ratio moduli of the synchrotron polarization intensity for Alfvén, slow, and fast modes.

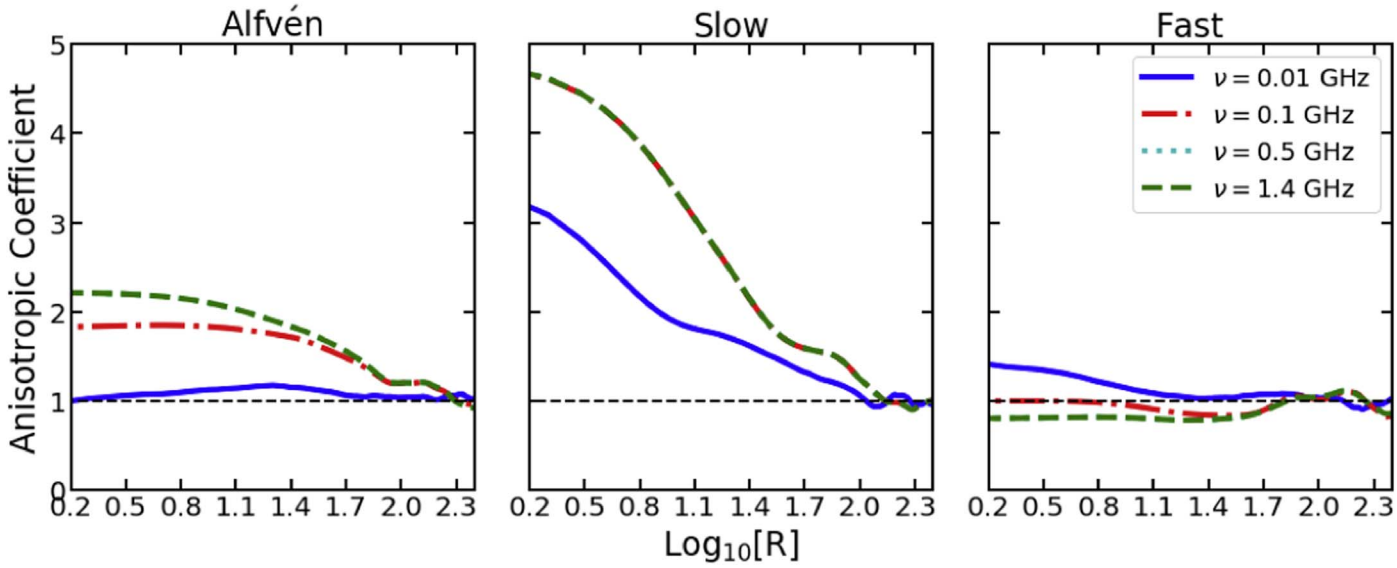

Figure 12. Influence of the radiation frequency on the anisotropic coefficients of the synchrotron polarization intensity for Alfvén, slow, and fast modes.

6. Discussion

This work studied the anisotropy of the synchrotron polarized intensity using a 2D normalized structure function, the quadrupole ratio modulus, and the anisotropic coefficient. The contour map of the structure function can qualitatively reveal the anisotropy of MHD turbulence, while the anisotropic coefficient adopting the ratio of the parallel component of the structure function to the perpendicular component can quantitatively measure the anisotropy. Importantly, the quadrupole ratio modulus can accurately reflect the degree of anisotropy at different scales.

The structure function map can be used as a prior for diagnosing the anisotropy of the synchrotron polarization intensity. The synergy effect can be realized in the quantitative study of the anisotropy of synchrotron polarization intensity by the combination of the quadrupole ratio and the anisotropic coefficient. The former can be used to accurately measure the amplitude of the anisotropy with no reflection of the mean magnetic field direction. The latter reveals the degree of the anisotropy by the ratio of the parallel to perpendicular component of the structure function with the successful reflection of the mean magnetic field direction. Provided with the anisotropic coefficient greater than 1, the parallel component of the synchrotron polarization intensity is larger than the perpendicular component, and vice versa.

Based on multiple sets of data, we first tested in Section 4.2 the results obtained by Lee et al. (2019), who studied how the wavelength affects the anisotropy of the synchrotron polarized intensity. Then, we move to focus on the investigation of the anisotropy of MHD turbulence. Generally, the structures of polarized intensities from Alfvén and slow modes are found to be anisotropic, being aligned with the direction of the mean magnetic field, while those from fast modes are isotropic, with the tendency of being perpendicular to the direction of the mean magnetic field. The results from the above three modes are consistent with that from the direct numerical simulation

of CL02 and CL03, only with a slightly stronger anisotropy of the slow modes than that of Alfvén modes. Meanwhile, the slow mode simulation shows less dependence on the radiation frequency.

Therefore, more robust measurements of the magnetic field can be achieved by means of the synchrotron polarization statistics, which restored the MHD turbulence modes successfully. The distinct properties of each mode revealed in our simulation provide us the possibility to distinguish the different contributions they make in the real astrophysical environment. Complementary to the synchrotron gradients technique mentioned previously to map the 3D structure of the magnetic field, the application of the second-order normalized structure function, quadrupole ratio modulus, and anisotropic coefficient provides a more detailed analysis for the contribution of the compressible MHD turbulence modes.

As is shown in Figures 5, 6, 11, and 12, the anisotropic level of the polarization intensity is relatively low at the frequency of 0.01 GHz, which makes the low-frequency polarized intensity more challenging to reveal the properties of MHD turbulence in the effect of the relevant noise and strong Faraday rotation. If the effect of small-scale noise is removed, we expect an increase in the degree of anisotropy, which should be similar to the scenario for the application of the synchrotron polarization gradient techniques in the low-frequency range (Zhang et al. 2019a, 2019b). The quadrupole ratio modulus and anisotropic coefficient used in this paper are complementary techniques to the gradient measurement. With the high-resolution data currently available from the Low Frequency Array for radio astronomy and those in the future from the Square Kilometer Array, these techniques will have broader application prospects.

7. Summary

The polarized intensity anisotropy has been investigated in this paper using the statistical techniques of the normalized structure function, the quadrupole ratio, and the anisotropic coefficient to reveal the anisotropy of compressible MHD turbulence. We focused on studying how Mach numbers, spectral index, and radiation frequency affect the anisotropy of the polarized intensity and exploring how to obtain the anisotropy of eddies related to the direction of the mean magnetic field. The main results are briefly summarized as follows.

1. The anisotropy of the synchrotron polarization intensity is found to be influenced by several MHD turbulence regimes. The most significant anisotropy of the polarized intensity occurs in the sub-Alfvénic turbulence regime, in which a gradual change in anisotropy occurs in the supersonic regime with the increase of the spatial scale.
2. With decreasing frequency, the level of the anisotropy of the polarization intensity is reduced due to the Faraday rotation effect. This is no obstacle to studying the MHD turbulence anisotropy and tracing the mean magnetic field directions.
3. On the basis of basic MHD modes decomposed using the sub-Alfvénic data cubes, we have found that
   (a) the anisotropy of the polarized intensity structure from Alfvén modes can help better trace the direction of the mean magnetic field, with slight reliance on the electron spectral index and the radiation frequency
   (b) the polarized intensity structure from slow modes is also anisotropic, showing a stronger anisotropy than that from Alfvén modes. The anisotropy for slow modes has marginal dependence on the electron spectral index and frequency
   (c) the polarized intensity structure from fast modes is nearly isotropic. For fast modes, the influence of the electron spectral index and frequency on the structure of polarized intensity is insignificant.
4. The elongated structures of the polarized intensity from Alfvén and slow modes are aligned with the direction of the magnetic field. These findings are in good consistency with those from the earlier direct numerical simulations.
5. The normalized structure function, anisotropic coefficient, and quadrupole ratio modulus are very synergetic in studying the anisotropy of compressible MHD turbulence. The former two can reflect the direction of the mean magnetic field, and the latter can accurately obtain the degree of anisotropy.

We thank the anonymous referee for valuable comments, Alex Lazarian for useful discussion, and Christopher Herron for providing the python code to calculate quadrupole ratio modulus. J.F.Z. is thankful for the support from the National Natural Science Foundation of China (grant Nos. 11973035 and 11703020) and the Hunan Provincial Natural Science Foundation (grant No. 2018JJ3484). F.Y.X. acknowledges the support of the National Natural Science Foundation of China (grant No. U1731106). R.Y.W. and J.F.Z. are thankful for the support of the Guizhou Provincial Key Laboratory of Radio Astronomy and Data Processing (grant No. KF201803).

References

Armstrong, J. W., Rickett, B. J., & Spangler, S. R. 1995, ApJ, 443, 209
Beck, R., & Wielebinski, R. 2013, in Planets, Stars and Stellar Systems, Vol. 5 ed. T. D. Oswalt & G. Gilmore. (Dordrecht: Springer), 641
Brentjens, M., & de Bruyn, A. 2005, A&A, 441, 1217
Burkhart, B., Lazarian, A., & Gaensler, B. M. 2012, ApJ, 749, 145
Burn, B. J. 1966, MNRAS, 133, 67
Cho, J., & Lazarian, A. 2002, PhRvL, 88, 245001
Cho, J., & Lazarian, A. 2003, MNRAS, 345, 325
Cho, J., Lazarian, A., & Vishniac, E. T. 2002, ApJ, 564, 291
Cho, J., & Vishniac, E. T. 2000, ApJ, 539, 273
Dickey, J. M., Landecker, T. L., Thomson, A. J. M., et al. 2019, ApJ, 871, 106
Elmegreen, B. G., & Scalo, J. 2004, ARA&A, 42, 211
Ferrière, K. M. 2001, RvMP, 73, 1031
Fletcher, A., Beck, R., Shukurov, A., et al. 2011, MNRAS, 412, 2396
Gaensler, B. M., Haverkorn, M., Burkhart, B., et al. 2011, Natur, 478, 214
Ginzburg, V. L., & Syrovatskii, S. I. 1965, ARA&A, 3, 297
Goldreich, P., & Sridhar, S. 1995, ApJ, 438, 763
Hamaker, J. P., & Bregman, J. D. 1996, A&AS, 117, 161
Haverkorn, M. 2015, ASSL, 407, 483
Herron, C. A., Burkhart, B., Lazarian, A., et al. 2016, ApJ, 822, 13
Herron, C. A., Gaensler, B. M., Lewis, G. F., et al. 2018, ApJ, 853, 9
Iroshnikov, P. S. 1964, SvA, 7, 566
Jelić, V., de Bruyn, A. G., Pandey, V. N., et al. 2015, A&A, 583, A137
Kowal, G., & Lazarian, A. 2010, ApJ, 720, 742
Kraichnan, R. H. 1965, PhFl, 8, 1385
Lazarian, A. 2006, ApJL, 645, L25
Lazarian, A., & Pogosyan, D. 2012, ApJ, 747, 5
Lazarian, A., & Pogosyan, D. 2016, ApJ, 818, 178
Lazarian, A., & Vishniac, E. T. 1999, ApJ, 517, 700
Lazarian, A., & Yuen, K. H. 2018, ApJ, 865, 59
Lee, H., Cho, J., & Lazarian, A. 2019, ApJ, 877, 108
Lithwick, Y., & Goldreich, P. 2001, ApJ, 562, 279
Mac Low, M.-M., & Klessen, R. S. 2004, RvMP, 76, 125

Maron, J., & Goldreich, P. 2001, ApJ, 554, 1175
Matthaeus, W. H., Ghosh, S., Oughton, S., & Roberts, D. A. 1996, JGR, 101, 7619
McKee, C. F., & Ostriker, E. C. 2007, ARA&A, 45, 565
Narayan, R., & Medvedev, M. V. 2001, ApJL, 562, L129
Shebalin, J. V., Matthaeus, W. H., & Montgomery, D. 1983, JPlPh, 29, 525
Van Eck, C. L., Haverkorn, M., Alves, M. I. R., et al. 2017, A&A, 597, A98
Yan, H., & Lazarian, A. 2008, ApJ, 673, 942
Zhang, J.-F., Lazarian, A., Ho, K. W., et al. 2019a, MNRAS, 486, 4813
Zhang, J.-F., Lazarian, A., Lee, H., & Cho, J. 2016, ApJ, 825, 154
Zhang, J.-F., Lazarian, A., & Xiang, F.-Y. 2018, ApJ, 863, 197
Zhang, J.-F., Liu, Q., & Lazarian, A. 2019b, ApJ, 886, 63